ACS EARTH AND SPACE CHEMISTRY

Article

Cite This: ACS Earth Space Chem. 2019, 3, 29–38

http://pubs.acs.org/journal/aesccq

Comparison of Arsenate and Molybdate Speciation in Hydrogenetic Ferromanganese Nodules

Shitong Yang,*[,†] Soichiro Uesugi,[†] Haibo Qin,[‡] Masato Tanaka,[†] Minako Kurisu,[†] Chihiro Miyamoto,[†] Teruhiko Kashiwabara,[§] Akira Usui,[∥] and Yoshio Takahashi*[,†]

[†]Department of Earth and Planetary Science, Graduate School of Science, The University of Tokyo, 7-3-1 Hongo, Bunkyo-ku, Tokyo 113-0033, Japan

[‡]State Key Laboratory of Environmental Geochemistry, Institute of Geochemistry, Chinese Academy of Sciences, Guiyang, Guizhou 550081, People's Republic of China

[§]Japan Agency for Marine-Earth Science and Technology, 2-15 Natsushima-cho, Yokosuka, Kanagawa 237-0061, Japan

[∥]Geology Department, Kochi University, 2-5-1 Akebono, Kochi 780-8520, Japan

ABSTRACT: Marine ferromanganese oxides contain a large amount of trace elements, such as arsenic (As) and molybdenum (Mo). However, the host phases of tetrahedral AsO_4^{3-} and MoO_4^{2-} oxyanions therein have not been clearly identified thus far. In this work, we explored the mineralogical components of hydrogenetic (HG) ferromanganese nodules and compared the distribution behaviors of As and Mo. The X-ray diffraction (XRD) and X-ray absorption spectroscopy (XAS) analyses showed that the predominant manganese and iron phases were vernadite (δ-MnO_2) and ferrihydrite, respectively. According to the sequential extraction examination, both As and Mo were associated with the iron (oxyhydr)oxide phases. However, the XAS analyses indicated that As was retained by the ferrihydrite phase via double corner-shared complexation, while Mo was preferentially adsorbed on δ-MnO_2 via edge-shared complexation. The immobilization of As and Mo by HG ferromanganese samples was attributed to specific chemical binding (ΔG_{chem}) rather than Coulombic interaction (ΔG_{coul}) as proposed in previous studies. The comparison of Mo XAS spectra before and after extraction revealed the unreliability of the sequential extraction approach to determine the host phase of trace elements as a result of the potential readsorption risk. The different distribution trends of As and Mo were due to their disparate intrinsic properties (e.g., averaged dissociation constants of conjugate acids) and the diverse properties (i.e., surface site densify, adsorption equilibrium constant, and crystalline structure) of ferrihydrite and δ-MnO_2. These research findings would be significant for evaluating the geochemical behaviors and environmental fate of trace elements in marine systems.

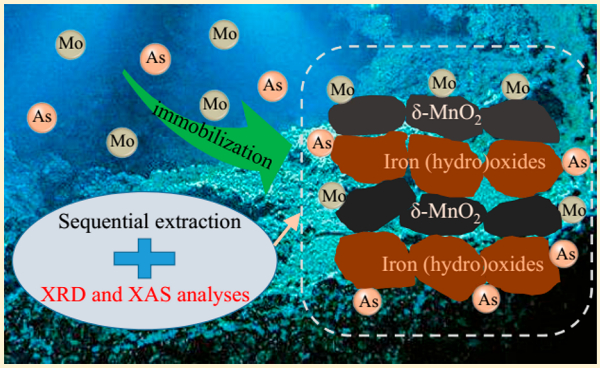

KEYWORDS: *sequential extraction, X-ray diffraction, X-ray absorption spectroscopy, readsorption risk, host phases, specific chemical binding, geochemical behaviors*

INTRODUCTION

Ferromanganese oxides, in the forms of hydrogenetic (HG) nodules or crusts, diagenetic (DG) nodules, and hydrothermal (HT) crusts as a result of different origins, are important chemical deposits in the marine environment. These aggregates of Fe (oxyhydr)oxides and Mn oxides greatly influence the distribution of various elements [e.g., lead (Pb), cobalt (Co), zinc (Zn), cerium (Ce), arsenic (As), antimony (Sb), tellurium (Te), molybdenum (Mo), tungsten (W), etc.] in seawater.[1−4] As and Mo are redox-sensitive trace metals, with their valence states and geochemical behaviors closely relevant to the redox conditions of seawater.[5] In the modern seawater under an aerobic environment, both of the two elements are present as the tetrahedral arsenate (AsO_4^{3-}) and molybdate (MoO_4^{2-}) oxyanions. However, the enrichment factor of As into the ferromanganese oxides was measured to be ca. 15 times higher than that of Mo.[6] In view of this, it is imperative to systematically understand the underlying immobilization mechanisms of As and Mo by ferromanganese oxides.

A series of analysis approaches have been adopted to verify the host phases of As and Mo in various ferromanganese samples of different deposition types and locations. For the HG and HT ferromanganese oxide samples from the Central Pacific, the sequential extraction data pointed to the preferential attachment of As on the $FeOOH{\cdot}xH_2O$ surfaces via electrostatic attraction.[7] With the aid of micro X-ray

Received: August 26, 2018
Revised: November 17, 2018
Accepted: December 6, 2018
Published: December 6, 2018

DOI: 10.1021/acsearthspacechem.8b00119
ACS Earth Space Chem. 2019, 3, 29–38

fluorescence (μ-XRF) mapping, X-ray diffraction (XRD), and X-ray absorption spectroscopy (XAS) analyses, Marcus et al. (2004) suggested that As was adsorbed on (via inner-sphere surface complexation) or co-precipitated with ferrihydrite in the DG ferromanganese samples collected from the Baltic Sea.[8] For the HT ferromanganese duricrusts obtained along the Yangtze River, the electron microprobe mapping and μ-XRF analyses revealed that As in the Fe-rich crusts was bound to the well-crystallized hematite phase via the bidentate binuclear linkage mode, while As in the Mn-rich samples was adsorbed on the pyrolusite surfaces by adopting the same complexation type.[9]

Similar to As, the spatial partitions of Mo among the iron and manganese minerals in natural ferromanganese oxides are also of high complexity and inconsistency. Previous XRF measurements and element correction analyses showed that Mo was associated with the Mn phase in the DG ferromanganese crusts collected from the Pacific Ocean.[10,11] However, on the basis of the sequential extraction results, it is suggested that Mo preferred to bind on the surfaces of amorphous iron oxyhydroxide in the HG ferromanganese nodules sampled from the Central Pacific. In contrast, Mo was immobilized by the manganese oxide phase in the HT ferromanganese precipitates obtained from the North Fiji Basin.[7] These conclusions on the host phases of Mo may be controversial as a result of the poor reproducibility and accuracy of the applied analysis methods. In our previous study, the Mo L_3-edge X-ray absorption near-edge structure (XANES) and K-edge extended X-ray absorption fine structure (EXAFS) techniques were used to provide insight into the microscopic speciation in the HG ferromanganese oxides collected from the Pacific Ocean.[12] The results indicated that Mo was associated with the amorphous MnO_2 phase via inner-sphere surface complexation. The obvious differences in the above-mentioned studies may originate from the disparate deposition types and mineralogical components of different ferromanganese oxides.

Although the distribution of individual As or Mo in various ferromanganese samples has been extensively explored,[7−12] no study is concentrated on comparing the host phases of these two elements in the same ferromanganese samples. Besides, the internal causes for their particular partitions are also poorly understood. For the purposes of filling in these knowledge gaps, we combined the sequential extraction approach, XRD, and XAS analyses to carefully identify the speciation of As and Mo in two HG ferromanganese nodules. First, the sequential extraction experiments were carried out to determine the concentrations of As and Mo in the ferromanganese samples. In addition, XRD, XANES, and EXAFS spectra were analyzed to identify the specific manganese and iron phases in the HG ferromanganese nodules. Moreover, the host phases and microscopic speciation of As and Mo were confirmed on the basis of XANES and EXAFS analyses. Furthermore, the distribution trends of As and Mo were compared and explained in detail.

EXPERIMENTAL SECTION

Sample Collection and Characterization. Two HG ferromanganese nodules were collected from the Pacific Ocean, i.e., AD14 around the Marshall Islands and D535 in the South Pacific Ocean.[2,3,12] The obtained samples were vacuum-dried and ground into powder by an agate mortar. In our previous studies,[2,3,12] the collected ferromanganese samples were digested using the combination of HF/HCl/HNO_3 and the elemental concentrations were determined with inductively coupled plasma mass spectrometry (ICP−MS, Agilent 7700). On the basis of the bulk chemical analyses, the concentrations of As and Mo in AD14 were ∼194 and ∼469 mg/kg, respectively, and those in D535 were ∼157 and ∼289 mg/kg, respectively.[2,3,12] The XRD patterns of AD14 and D535 were scanned by a RIGUKA diffractometer (RINT-2100) equipped with Cu Kα (λ = 1.5406 Å) radiation (40 kV voltage and 20 mA cathodic current). The scanning range was from 5° to 70°, and the scanning step was 0.02°.

A series of manganese oxides [i.e., triclinic birnessite and vernadite (δ-MnO_2)] and Fe (oxyhydr)oxides (i.e., magnetite, ferrihydrite, goethite, and hematite) were synthesized by following the strategies reported in the previous literature.[13−15] In addition, the Mo and As adsorption samples [i.e., Mo(VI) on δ-MnO_2, Mo(VI) on ferrihydrite, Mo(VI) on goethite, Mo(VI) on hematite, As(V) on δ-MnO_2, and As(V) on ferrihydrite] were also prepared as the reference samples. The detailed experimental conditions and procedures were described in our previous study.[12]

Sequential Extraction Experiments. The concentrations and fractions of Mn, Fe, As, and Mo in our ferromanganese samples were measured by adopting the previously reported sequential extraction procedures.[1,7,16] First, 0.5 g of powdered sample was soaked in 15.0 mL of acetic acid/sodium acetate buffer (pH 5.0), and the resulting suspension was gently stirred for 5 h (denoted as leach 1). The filtrate contained those of As and Mo adsorbed via weak electrostatic interaction or retained by calcium carbonates. The residue was then mixed with 87.5 mL of hydroxylamine hydrochloride solution (0.1 mol/L, pH 2.0), and the suspension was oscillated for 24 h (denoted as leach 2). During this leaching procedure, the amorphous manganese oxides would dissolve, and accordingly, As and Mo associated with this mineral phase would be released into the solution. The residue of leach 2 was soaked in 87.5 mL of oxalic acid/ammonia oxalate buffer (0.2 mol/L, pH 3.5) and stirred for 12 h (denoted as leach 3). The filtrate of this leaching step contained those of As and Mo immobilized by the moderately reducible iron oxyhydroxide phases. The filtrates in each leaching step were diluted using 2% HNO_3 solution, and the concentrations of Mn and Fe were determined by inductively coupled plasma atomic emission spectrometry (SP3500, SII Nano Technology, Inc.). The concentrations of As and Mo were measured by ICP−MS. According to the previous studies, the main components in the residue after leach 3 were identified to be the hardly soluble silicates and aluminosilicates.[1,7,16] The concentrations of Mn, Fe, As, and Mo sequestrated by these phases (denoted as residual) were calculated by adopting the indirect subtractive method (i.e., the total concentrations determined from the bulk chemical analyses subtract those measured in leach steps 1−3).

XAS Data Measurement and Analysis. Manganese (Mn), iron (Fe), and arsenic (As) K-edge XANES and EXAFS spectra were measured at BL01B1 of SPring-8 (Japan) with a Si(111) double-crystal monochromator. The Mn- and Fe-containing standard, adsorption, and natural ferromanganese samples were measured in transmission mode. The As-containing adsorption and ferromanganese samples were measured in fluorescence mode using a 19-element Ge solid-state detector. Mo L_3-edge XANES spectra were collected at BL9A in the Photon Factory, High Energy Accelerator

DOI: 10.1021/acsearthspacechem.8b00119
ACS Earth Space Chem. 2019, 3, 29−38

Research Organization (KEK, Japan) with a Si(111) monochromator. The MoO_4^{2-} solution (0.10 mol/L) was measured in transmission mode. The Mo-containing adsorption samples and ferromanganese nodules were measured in fluorescence mode using a Lytle detector.

All of the measured spectra were analyzed with the aid of Athena and Artemis software.[17] The k^3-weighted EXAFS oscillations were extracted from the raw data and Fourier-transformed to obtain the corresponding radical structural functions (RSFs). Further spectral fits were performed by adopting the nonlinear least squares approach. With the aid of FEFF 8.0,[18] the theoretical phase shifts and amplitude functions for the As−O, As−Fe, and As−Mn paths were extracted from the crystalline structures of scorodite ($FeAsO_4 \cdot 2H_2O$) and manganese arsenate hydrate ($MnAsO_4 \cdot H_2O$).

RESULTS AND DISCUSSION

Sequential Extraction Data Analyses. The relative proportions (%) of Mn, Fe, As, and Mo leached from the HG ferromanganese samples of AD14 and D535 are shown in the form of a stacked bar chart (Figure 1). Specifically for

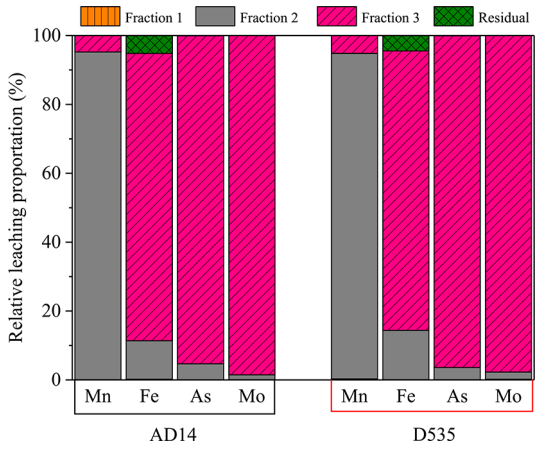

Figure 1. Leaching percentages of Mn, Fe, As, and Mo from the natural ferromanganese samples AD14 and D535 within the sequential extraction procedures.

AD14, almost no Mn, Fe, As, and Mo are desorbed in leach 1 using acetic acid/Na acetate buffer as the eluent. This result suggests that these four elements are neither present as the exchangeable species nor retained in the Ca carbonate mineral. The absence of exchangeable species is reasonable as a result of the inhibition of high ionic strength in seawater toward their sorption behaviors. Leach 2 (hydroxylamine hydrochloride extraction) releases ∼95% of total Mn, ∼11% of total Fe, ∼5% of total As, and ∼2% of total Mo. Herein, the released Fe may represent the iron phase intergrowth with the δ-MnO_2 mineral in the HG crusts.[1,7,16] Subsequent leach 3 with oxalic acid/ammonia oxalate treatment dissolves ∼5% of total Mn, ∼84% of total Fe, ∼95% of total As, and up to ∼98% of total Mo. According to the indirect subtractive calculation, ∼5% of total Fe is associated with the hardly soluble silicates and/or aluminosilicates. The relative leaching proportions of Mn, Fe, As, and Mo from D535 are comparable to those from AD14 (Figure 1), suggesting the similar components of these two ferromanganese crusts from the same HG origin.

According to the anticorrelation of As and Mo with Mn and their positive correlation with Fe, it seems that these two elements are chemically bound to iron oxyhydroxide rather than manganese oxide. However, this conclusion may be controversial as a result of the potential readsorption risk as reported in a series of sequential extraction studies.[1,19,20] On the basis of the radiochemical analyses, Gilmore et al. (2001) proposed that ∼35−85% Pb leached from the reducible Fe and Mn oxides was readsorbed by the oxidizable organics and sulfides.[20] In addition, our previous study based on ^{139}Ce and ^{146}Gd isotope tracer measurements also indicated that ∼35% Ce and ∼46% Gd leaching from the Mn phase were readsorbed onto Fe (oxyhydr)oxide during the hydroxylamine hydrochloride extraction procedure.[2] Similarly, the readsorption of As and Mo may also occur in our sequential extraction experiments. Therefore, additional analysis approaches should be adopted to clearly identify the host phases of As and Mo in the ferromanganese samples.

Manganese and Iron Phases in Natural Ferromanganese Crusts. XRD analysis is a useful approach to identify the Mn and Fe (oxyhydr)oxide phases in the ferromanganese samples. One can see from Figure 2 that AD14 and D535 with

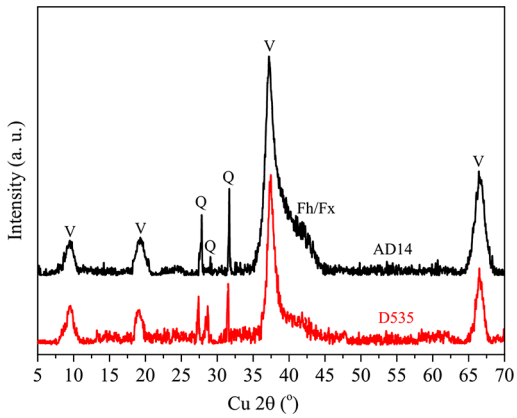

Figure 2. XRD patterns of ferromanganese nodules. Diffraction peaks labeled V, Q, and Fh/Fx refer to vernadite, quartz, and ferrihydrite/feroxyhite, respectively.

HG origin exhibit similar XRD patterns. Specifically, the diffraction peaks at ∼9.7°, ∼19.3°, ∼37.2°, and ∼66.5° correspond to the (001), (002), (100), and (110) planes of Fe−vernadite (δ-MnO_2, marked by V).[21,22] The sharp diffraction peaks at ∼27.5°, ∼28.4°, and ∼31.6° correspond to the quartz impurity (marked by Q). The broad diffraction peak centered at ∼42.5° points to the presence of ferrihydrite and/or feroxyhite (δ-FeOOH) phases (marked by Fh/Fx).[22−25] According to the previous selected area electron diffraction (SAED), energy-dispersive spectroscopy (EDS), and Mössbauer spectroscopy analyses, the Fe−vernadite phase in the marine ferromanganese nodules exhibited a hybrid structure as a result of the intergrowth of feroxyhite with δ-MnO_2.[24,26,27] In addition, the epitaxial intergrowth of the iron phase may disrupt the stacking of manganese layers.[22] This intergrowth mechanism is supported by the relatively weak (001) and (002) basal reflections of the Fe−vernadite phase. Overall, the XRD analysis results herein are consistent with those derived from sequential extraction data (Figure 1).

The K-edge XANES and EXAFS spectra of Mn-containing reference components (i.e., Mn_2O_3, triclinic birnessite, and δ-MnO_2) and ferromanganese samples (i.e., AD14 and D535) are compared to further verify the average oxidation state

DOI: 10.1021/acsearthspacechem.8b00119
ACS Earth Space Chem. 2019, 3, 29−38

(AOS) and predominant mineral phase of Mn. Specifically, the XANES spectrum of Mn_2O_3 with the Mn AOS of 3.0 exhibits a broad X-ray absorption peak centered at 6553.9 eV (marked by the dashed line in Figure 3). In contrast, the spectrum of

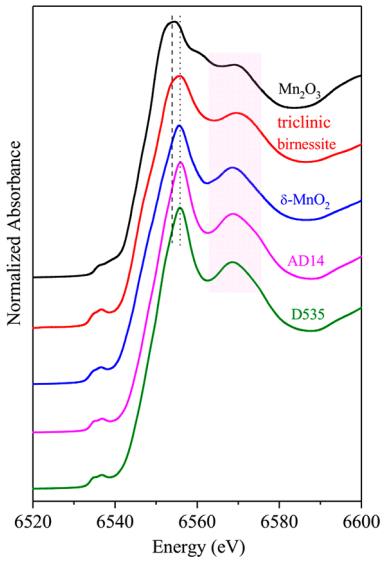

Figure 3. XANES spectra of Mn-containing reference samples and ferromanganese nodules.

triclinic birnessite shows a main absorption peak at 6555.8 eV (marked by the dotted line in Figure 3) and a weak shoulder at a lower energy of 6553.9 eV, indicating the presence of mixed Mn oxidation states of +3 and +4 in its crystalline structure. The XANES spectrum of δ-MnO_2 with Mn AOS close to 4.0 exhibits a sharp absorption peak at 6555.8 eV (marked by the dotted line in Figure 3). As for the spectra of AD14 and D535, both the position and shape of the main absorption peak at 6555.8 eV (marked by the dotted line) and the second peak within 6563.5−6578.4 eV (marked by the rectangle) are extremely similar to that of δ-MnO_2, while obviously different from those of Mn_2O_3 and triclinic birnessite. One can preliminarily conclude that δ-MnO_2 is the primary Mn mineral in our HG ferromanganese samples.

Figure 4 illustrates the k^3-weighted EXAFS spectra (A) and the Fourier-transformed RSFs (B) of Mn-containing samples. Specifically, the $k^3\chi(k)$ spectrum of δ-MnO_2 shows two sharp peaks at ∼8.00 and ∼9.10 $Å^{-1}$ (see the dashed lines in Figure 4A), while that of triclinic birnessite exhibits an apparent peak splitting at ∼8.00 $Å^{-1}$ and a broad peak centered at ∼8.90 $Å^{-1}$ (left shift relative to that of δ-MnO_2). These spectral differences were previously interpreted from the different AOS of Mn and the disparate symmetry of MnO_6 layers in the crystalline structures of δ-MnO_2 and triclinic birnessite.[8,28,29] The δ-MnO_2 phase has a hexagonal MnO_6 symmetry with a certain amount of vacant sites as well as an extremely low content and low ordering of Mn(III).[28,29] Triclinic birnessite possesses an orthogonal MnO_6 symmetry with no vacant sites as well as a relatively high content (∼33%) and high ordering of Mn(III).[30] Under such circumstances, the enrichment and ordering of Mn(III) in triclinic birnessite lead to the peak splitting, broadening, and shifting in the $k^3\chi(k)$ spectrum. As shown in Figure 4A, the k^3-weighted EXAFS spectra of AD14 and D535 are similar to that of δ-MnO_2, suggesting that δ-MnO_2 is the predominant Mn phase in our ferromanganese

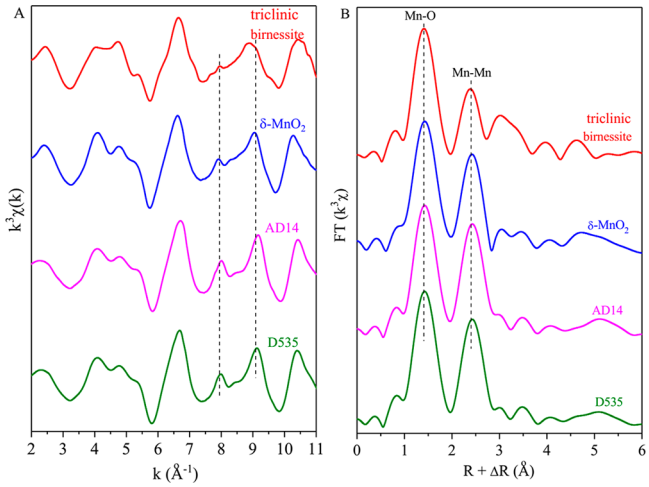

Figure 4. (A) k^3-weighted EXAFS spectra and (B) corresponding RSFs of Mn-containing reference samples and ferromanganese nodules.

samples. It is worth noting that the $k^3\chi(k)$ spectrum of δ-MnO_2 is comparable to that of H−birnessite, another kind of manganese oxide with hexagonal symmetry.[29] In view of this, one cannot eliminate the potential presence of H−birnessite in the ferromanganese nodules solely based on the oscillation characteristics in the $k^3\chi(k)$ spectra. Nevertheless, the spectral features in the RSFs can provide more information to further identify the main manganese phase. Herein, all of the RSFs (phase shift uncorrected) exhibit two dominant peaks at ∼1.40 Å (corresponding to the Mn−O shell) and ∼2.40 Å (corresponding to the edge-shared Mn−Mn shell) (see the dashed lines in Figure 4B). It was reported that the relative intensity ratio of these two peaks (I_{Mn-Mn}/I_{Mn-O}) was negatively correlated to the occupation fraction of layer vacancy sites by Mn(III) (f_{occ}).[28,29,31] Herein, the calculated I_{Mn-Mn}/I_{Mn-O} values of δ-MnO_2 (0.83), AD14 (0.92), and D535 (0.89) are higher than that of triclinic birnessite (0.66), while lower than that of H−birnessite (1.01) reported in the previous study.[29] Therefore, one can definitely conclude that the primary manganese phase in the ferromanganese nodules is δ-MnO_2 rather than triclinic birnessite or hexagonal H−birnessite.

The above sequential extraction data indicate that the iron phases in our hydrogenetic ferromanganese samples are potentially present in three different forms, i.e., Fe−vernadite (feroxyhite intergrowth with δ-MnO_2), iron (oxyhydr)oxides, and structural association with (alumino)silicates. The previous SAED pattern and Fe K-edge EXAFS spectra showed that the microstructure of Fe−vernadite was extremely similar to that of feroxyhite.[24,26] On the basis of the Fourier-transformed RSFs, EXAFS-derived Fe−Fe distances, and the static disorder analyses, previous researchers proposed that the local structure of feroxyhite resembled that of hematite while different from those of ferrihydrite and goethite.[24,27] As for the iron species in (alumino)silicates, previous molecular dynamics (MD) calculations, ^{57}Fe Mössbauer spectroscopy, and powder and polarized EXAFS analyses suggested the incorporation of Fe^{3+} into the MgO_6/AlO_6 octahedral layers.[32,33] Herein, the XANES and EXAFS spectra of Fe-containing reference samples and natural ferromanganese crusts (AD14 and D535) are analyzed to further identify the coordination environment of iron.

DOI: 10.1021/acsearthspacechem.8b00119
ACS Earth Space Chem. 2019, 3, 29−38

The XANES spectrum of magnetite (Fe_3O_4) with the mixed Fe oxidation states of +2 and +3 exhibits a sharp X-ray absorption peak at 7126.2 eV (marked by the dashed line in Figure 5A), while the absorption peaks of goethite, hematite, and ferrihydrite with a pure Fe oxidation state of +3 are located at a higher energy of 7129.7 eV (marked by the dotted line in Figure 5A). Nevertheless, some small differences can be also observed between their XANES spectra. Specifically, the absorption peak of goethite is somewhat broader than those of hematite and ferrihydrite. For hematite, a small bulge appears at the left side of the main adsorption peak. In contrast, the absorption peak of ferrihydrite is smoother than those of goethite and hematite. As shown in Figure 5A, the XANES spectral features of AD14 and D535 are very similar to that of ferrihydrite. In view of this, the predominant iron phase in the HG ferromanganese samples can be identified to be amorphous ferrihydrite. This conclusion is further supported by the similarity between the $k^3\chi(k)$ EXAFS spectra of AD14, D535, and ferrihydrite (Figure 5B). However, we cannot fully eliminate the presence of other iron-bearing phases based merely on the intuitive spectral observations. In view of this, the linear combination fitting (LCF) on the $k^3\chi(k)$ spectra (within the k range of 3−11) of AD14 and D535 is performed using ferrihydrite, goethite, and hematite as the standards. The iron component incorporated into the structure of (alumino)-silicates is not considered as a result of its extremely low proportion (<5%; Figure 1). During the LCF processes, all standards are set to share the same E_0 value and the total weights are forced to sum to 100%. Specifically, AD14 contains ~86% ferrihydrite, ~10% hematite (or feroxyhite with a similar structure as indicated above), and ~4% goethite. Similarly, the relative proportions of ferrihydrite, hematite (or feroxyhite), and goethite in D535 are ~84%, ~11%, and ~5%, respectively. These simulation results are consistent with those derived from the sequential extraction experiments (Figure 1).

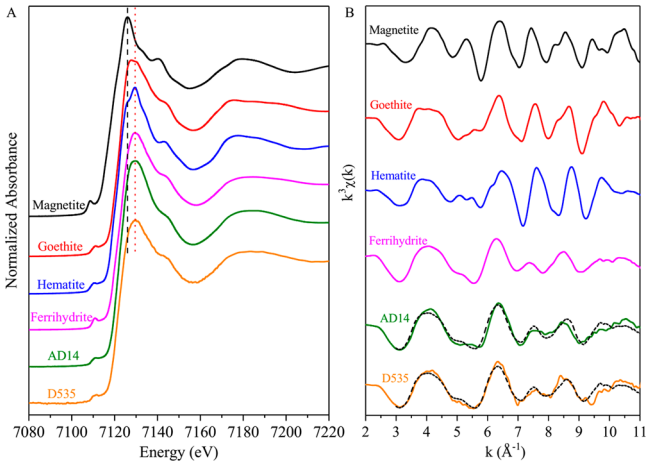

Figure 5. (A) XANES and (B) k^3-weighted EXAFS spectra of Fe-containing reference samples and ferromanganese nodules. Solid lines represent the experimental spectra, and dashed lines represent the least squares fit curves.

Coordination Environment of As and Mo. The K-edge XANES and EXAFS spectra of As-containing reference components [i.e., $KAsO_2$ as As(III) standard and KH_2AsO_4 as As(V) standard], adsorption samples (i.e., As(V) on δ-MnO_2 and As(V) on ferrihydrite), and ferromanganese nodules (i.e., AD14 and D535) are analyzed to identify the oxidation state and host phase of As. Specifically, the XANES spectrum of $KAsO_2$ with the As oxidation state of +3 exhibits a sharp X-ray absorption peak at 11 864.5 eV (dashed line in Figure 6). In contrast, the spectra of KH_2AsO_4, As(V) on δ-MnO_2, As(V) on ferrihydrite, AD14, and D535 show a sharp absorption peak at a higher energy of 11 867.6 eV (dotted line in Figure 6). This phenomenon indicates that As is present in the higher oxidation state of +5 in our ferromanganese samples.

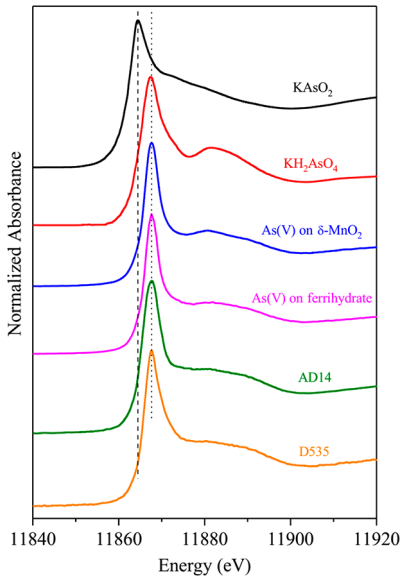

Figure 6. XANES spectra of As-containing reference samples and ferromanganese nodules.

EXAFS analyses can provide more detailed information to further confirm the retention mechanisms of As. Figure 7A shows the k^3-weighted EXAFS spectra of As-containing adsorption samples and natural ferromanganese oxides. The $k^3\chi(k)$ spectrum of As(V) on δ-MnO_2 exhibits a dished spectral feature within 7−8 Å^{-1} and a clear splitting at 9.5 Å^{-1} (marked by ellipses), similar to that of As(V) adsorbed on

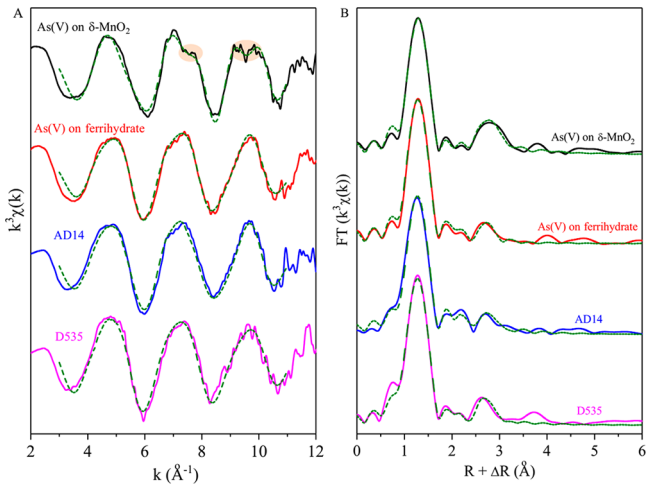

Figure 7. (A) k^3-weighted EXAFS spectra and (B) corresponding RSFs of As-containing reference samples and ferromanganese nodules. Solid lines represent the experimental spectra, and dashed lines represent the least squares fit curves.

DOI: 10.1021/acsearthspacechem.8b00119
ACS Earth Space Chem. 2019, 3, 29−38

Table 1. EXAFS-Derived Structural Parameters of Arsenate-Containing Reference Samples and Natural Ferromanganese Oxides[a]

sample	shell	CN	R (Å)	ΔE_0 (eV)	σ^2 (Å^2)	Res (%)
As(V) on δ-MnO_2	As−O	4.1	1.70	6.04	0.002	1.50
	As−O−O	1.2	3.09		0.002	
	As−Mn	1.5	3.20		0.006	
As(V) on ferrihydrate	As−O	4.0	1.71	5.68	0.003	1.93
	As−O−O	12	3.08		0.003	
	As−Fe	1.3	3.30		0.005	
AD14	As−O	4.2	1.70	5.47	0.004	2.67
	As−O−O	12	3.11		0.004	
	As−Fe	1.4	3.31		0.009	
D535	As−O	4.0	1.71	5.81	0.003	2.54
	As−O−O	12	3.10		0.003	
	As−Fe	1.6	3.30		0.008	

[a]CN, coordination number; R, interatomic distance; ΔE^0, difference between the experimental and FEFF calculated threshold energies; σ^2, Debye−Waller factor; and Res, deviation between the experimental and theoretical EXAFS curves. σ^2_{As-O-O} is constrained to be equal to σ^2_{As-O} during the spectral fit procedures.

synthetic birnessite.[34] In contrast, the EXAFS spectrum of As(V) on ferrihydrite shows uniform sinusoidal oscillation signals within the whole k range, which is obviously different from that of As(V) on δ-MnO_2. More specifically, the near symmetrical spectral feature at 4−6 Å^{-1} suggests that As is immobilized by ferrihydrite via the inner-sphere complexation mechanism.[35,36] The potential precipitation of ferric arsenate ($FeAsO_4{\cdot}4{-}7H_2O$) and scorodite ($FeAsO_4{\cdot}2H_2O$) phases can be further eliminated as a result of the absence of their characteristic double-hump feature.[37] The $k^3\chi(k)$ spectra of As in AD14 and D535 are similar to that of As(V) on ferrihydrite, suggesting that this element is predominantly enriched by the ferrihydrite phase in the natural ferromanganese nodules. Nevertheless, we cannot fully rule out the possibility that a small amount of As is also adsorbed onto the δ-MnO_2 surfaces, as indicated by the above sequential extraction data (Figure 1).

The k^3-weighted EXAFS data are Fourier-transformed to generate the corresponding RSFs (phase shift uncorrected). As shown in Figure 7B, all of the samples exhibit a sharp and intensive peak at $R + \Delta R \sim 1.30$ Å, which corresponds to the backscattering signals of O atoms surrounding the central As. In addition, a wide peak ranging from $R + \Delta R = 2.34$ to 3.50 Å appears in the RSF of As(V) on δ-MnO_2, suggesting the presence of a higher coordination shell (e.g., As−Mn). Similarly, the appearance of a narrow peak within $R + \Delta R =$ 2.32−3.05 Å for As(V) on ferrihydrite, AD14, and D535 points to the potential contribution of As−Fe paths to the RSFs of these samples. The structural parameters obtained from the least squares fits of EXAFS spectra are listed in Table 1. For all of the samples, the As−O interatomic distance (R_{As-O}) of ∼1.70 Å and coordination number (CN_{As-O}) of ∼4.0 in the first shell suggest an AsO_4 tetrahedral configuration. The As−O−O path with R_{As-O-O} of ∼3.10 Å and CN_{As-O-O} of 12 corresponds to the multiple scattering of O−O pairs in the AsO_4 tetrahedra.[38−40] The specific binding modes of As on different minerals can be further determined from the R and CN values of the As−Mn/Fe bonds. For As(V) on δ-MnO_2, the presence of 1.5 Mn atoms at R_{As-Mn} of ∼3.20 Å points to the formation of inner-sphere surface complexes in the double corner-shared (^{2}C) mode.[41,42] The EXAFS-derived structural parameters of AD14 and D535 (i.e., $R_{As-Fe} \sim 3.30$ Å and $CN_{As-Fe} \sim 1.5$) are similar to that of As(V) on ferrihydrite, representing the double corner-shared (DCS) complexation between AsO_4 tetrahedra and FeO_6 octahedra as predicted by previous density functional theory (DFT) calculations and EXAFS analyses.[35,43−46] The result herein implies that the ferrihydrite mineral is the host phase for the immobilization of As.

The local structures of Mo in the reference samples and ferromanganese nodules can also be identified from the XAS analyses as reported in our previous study.[12] Specifically, the L_3-edge XANES spectra of all samples exhibit two peaks within 2519−2527 eV (Figure 8),[12] of which the relative intensities

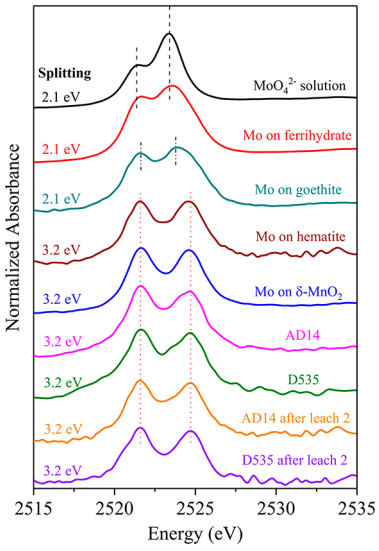

Figure 8. XANES spectra of Mo-containing reference samples and ferromanganese nodules.

and energy splitting reflect the specific coordination environment of Mo. According to the detailed discussion in our previous work,[12] Mo was adsorbed by ferrihydrite in the tetrahedral (Td) MoO_4 form, similar to the dissolved MoO_4^{2-} ions. In contrast, the species of Mo on δ-MnO_2 is in the octahedral (Oh) MoO_6 symmetry, suggesting the transformation of Mo species from Td to Oh during its sorption process. The XANES spectral features of AD14 and D535 are extremely similar to those of Mo on δ-MnO_2 and hematite while significantly different from that of Mo on ferrihydrite.

DOI: 10.1021/acsearthspacechem.8b00119
ACS Earth Space Chem. 2019, 3, 29−38

One can preliminarily deduce that Mo is possibly immobilized by δ-MnO_2/hematite rather than ferrihydrite. The specific host phase can be clearly identified on the basis of our previous EXAFS analyses.[12] Specifically, the $k^3\chi(k)$ spectra and the corresponding RSFs of AD14 and D535 are identical to that of Mo on δ-MnO_2 while distinct from those of Mo on ferrihydrite, goethite, and hematite. These results suggest that the predominant host phase of Mo is δ-MnO_2 rather than iron (oxyhydr)oxides. In addition, the presence of 2.0 Mn atoms at R_{Mo-Mn} of 3.02 Å points to a bidentate edge-shared (ES) linkage of distorted MoO_6 with the MnO_6 octahedra.[12]

The XAS analysis results derived herein are contrary to that obtained from the sequential extraction experiments (see Figure 1). To find the internal cause for this inconsistence, we carefully compare the XANES spectra of AD14 and D535 before extraction and after leaching 2. As shown in Figure 8, the spectra after extraction are very similar to those of Mo on hematite (or feroxyhite with a similar local structure) and δ-MnO_2 while different from those of Mo on ferrihydrite and goethite. Considering that δ-MnO_2 is completely dissolved by hydroxylamine hydrochloride during leach 2, the XANES spectrum suggests that Mo is adsorbed on the residual hematite (or feroxyhite) phase. In addition, the EXAFS analyses clearly show that the original host phase of Mo in AD14 and D535 is not hematite (or feroxyhite) but δ-MnO_2.[12] According to these direct spectral evidence, it seems that the Mo species leached from δ-MnO_2 are readsorbed onto hematite (or feroxyhite). Note that Mo prefers to bind on the minor hematite (or feroxyhite) phase (~11%) rather than the predominant ferrihydrite phase (~85%). This phenomenon can be tentatively interpreted by considering the binding mechanisms of Mo on different iron minerals and the relative stabilities of the sorption species. On the basis of our previous EXAFS analyses,[12] the predominant sorption mechanisms of Mo on ferrihydrite and hematite were proposed to be outer-sphere and inner-sphere complexations, respectively. In general, the outer-sphere complexes, similar to the aqueous species, can be easily released from the mineral surfaces as a result of the weak Coulombic interaction.[44,45] In contrast, the inner-sphere surface complexes tend to be stable and irreversible as a result of the formation of a strong covalent linkage.[47,48] Hence, it is reasonable that desorbed Mo from the δ-MnO_2 phase would be preferentially adsorbed by hematite (or feroxyhite) rather than ferrihydrite. This potential readsorption risk induces the uncertainty of the sequential extraction method for identifying the actual host phase of Mo. Alternatively, the combination of advanced spectroscopic techniques (e.g., XANES and EXAFS adopted in this work) with a sequential extraction approach can provide more reliable information on the real distribution and speciation of Mo and As in the Fe−Mn nodules.

Comparison of the Distribution of As and Mo. In our HG ferromanganese samples, As is selectively retained by the ferrihydrite phase via the DCS binding mode, while Mo is adsorbed on δ-MnO_2 surfaces via the ES linkage mode. Generally, the change in the total Gibbs free energy (ΔG_{ads}) during the adsorption of dissolved ions on metal (hydro)oxides can be described by the following equation:[49]

$$\Delta G_{ads} = \Delta G_{coul} + \Delta G_{sol} + \Delta G_{chem} \quad (1)$$

where ΔG_{coul} and ΔG_{chem} represent the free energies of Coulombic interaction and specific chemical interaction between the ions and oxide surfaces, respectively, while ΔG_{sol} is the free energy of solvation (hydration). According to this equation, the surface charges of manganese and iron-containing minerals in the natural ferromanganese oxides would influence the immobilization of trace elements, such as As and Mo, through ΔG_{coul}. The point of zero charge (pH_{pzc}) values of δ-MnO_2, ferrihydrite, hematite (or feroxyhite), and goethite were reported be 2.8−4.5, 7.9−8.7, 7.5−8.8, and 8.5−9.5, respectively.[50] Under the deep-ocean conditions with an average pH value of 8.0,[7] the surfaces of δ-MnO_2 would be negatively charged, while the three iron-containing minerals would have a slightly positive charge. For a series of studies involving the distribution of different elements in marine ferromanganese samples, it was commonly recognized that cations, such as Pb^{2+}, Zn^{2+}, and Ni^{2+}, were preferentially immobilized by manganese oxides with a negative surface charge, while oxyanions, such as MoO_4^{2-}, AsO_4^{3-}, and WO_4^{2-}, tended to be adsorbed on the positively charged Fe (hydr)oxide surfaces.[4,51] However, according to our EXAFS analyses, the host phase for the negative charge MoO_4^{2-} species is negatively charged δ-MnO_2 rather than positively charged ferrihydrite.[12] This phenomenon leads to new insight into the importance of ΔG_{chem} (i.e., specific chemical binding) for the enrichment of Mo by ferromanganese oxides. Despite the presence of electrostatic attraction between AsO_4^{3-} and ferrihydrite surfaces, the formation of inner-sphere surface complexes also highlights the important role of ΔG_{chem} in the immobilization of As by ferromanganese nodules. This is consistent with the absence of ion-exchangeable As and Mo species (Figure 1), showing that ΔG_{coul} is actually not very important for their sorption to the ferromanganese oxides under high-salinity conditions in seawater.

The specific binding modes (i.e., outer-sphere or inner-sphere surface complexation) of oxyanions on iron (oxyhydr)-oxides are closely associated with the averaged proton dissociation constants [$p\bar{K}_a = (pK_{a_1} + pK_{a_2})/2$] values of their conjugate acids. Previous studies proposed that WO_4^{2-} ($p\bar{K}_a$ = 3.92 for H_2WO_4) tended to form bidentate inner-sphere complexes on ferrihydrite surfaces via two oxygen atoms surrounding the center W atom.[2,52] More specifically, the MoO_4^{2-} oxyanion with the $p\bar{K}_a$ value of H_2MoO_4 lower than that of H_2WO_4 was expected to be adsorbed by ferrihydrite via outer-sphere complexation. In contrast, the $HAsO_4^{2-}$ oxyanion with the $p\bar{K}_a$ value of H_3AsO_4 higher than that of H_2WO_4 preferred to form inner-sphere surface complexes on ferrihydrite. These theoretical predictions of Mo(VI) and As(V) surface complexes on ferrihydrite are consistent with the foregoing EXAFS analysis results. In addition, the affinities of oxyanions for binding on the mineral surfaces are also dependent upon the stabilities of sorption species. As discussed above, inner-sphere surface complexes are relatively more stable than outer-sphere complexes.[47,48] In view of this, Mo(VI) would prefer to interact with δ-MnO_2 in the ferromanganese nodules and form stable inner-sphere complexes.

The preferential binding behavior of As onto ferrihydrite rather than δ-MnO_2 can be interpreted from the surface properties of iron and manganese (oxyhydr)oxides and the stability of the surface-adsorbed species. A previous surface complexation modeling showed that the surface site density of goethite (0.81 sites nm^{-2}) was higher than that of birnessite (0.45 sites nm^{-2}).[53] More importantly, the adsorption equilibrium constants of As(V) on the active sites of goethite

DOI: 10.1021/acsearthspacechem.8b00119
ACS Earth Space Chem. 2019, 3, 29−38

Table 2. Local Structure of AsO_4 Tetrahedra Adsorbed on Ferrihydrite Surfaces and FeO_4 Tetrahedra in the Crystalline Lattice of Ferrihydrite

	first neighboring shell			second neighboring shell			third neighboring shell		
coordination geometry	bond	CN	R (Å)	bond	CN	R (Å)	bond	CN	R (Å)
AsO_4 tetrahedra on ferrihydrite	As−O	4.0	1.71	As−O−O	12	3.08	As−Fe	1.3	3.30
FeO_4 tetrahedra in ferrihydrite	Fe−O	4.0	1.91	Fe−O−O	3.0	3.11	Fe−Fe	10.0	3.38

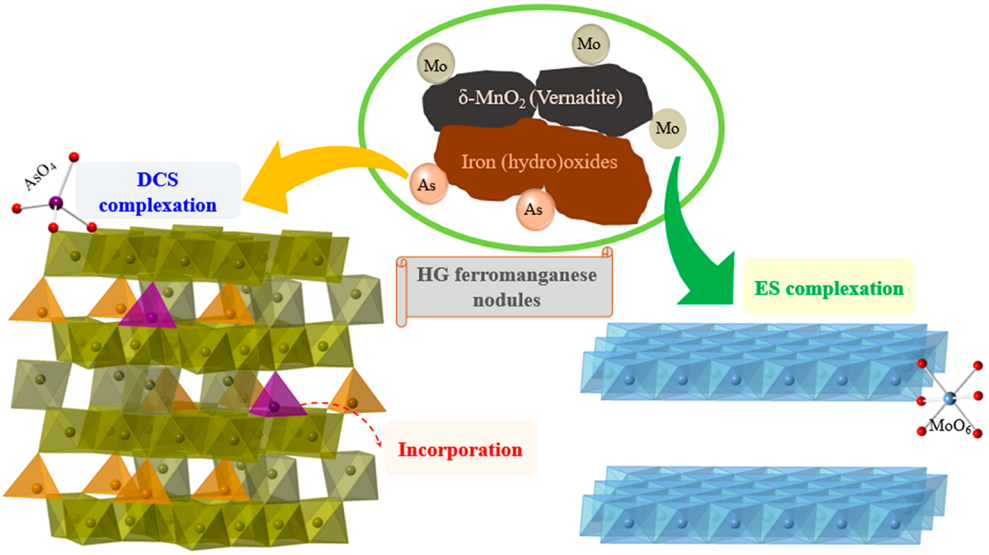

Figure 9. Schematic illustration on the potential immobilization mechanisms of As and Mo by HG ferromanganese nodules.

were much higher than those on the binding sites of birnessite.[53] It was reported that ferrihydrite had a bigger surface area, greater surface site density, and higher Se(IV) sorption capacity than goethite.[54] By consideration of the similar sorption mechanisms of As(V) and Se(IV) on the Fe and Mn (oxyhydr)oxides,[55,56] one can expect that As(V) would be preferentially immobilized by ferrihydrite rather than δ-MnO_2 in the HG ferromanganese nodules.

In addition to the surface properties, the unique crystalline structure of ferrihydrite may also contribute to the preferential binding of As(V). Previous real-space simulation of the pair distribution function suggested that the ideal ferrihydrite structure was composed of 80% FeO_6 octahedra and 20% FeO_4 tetrahedra.[57] Herein, the presence of FeO_4 tetrahedra may provide the potential opportunity for the lattice substitution of AsO_4 tetrahedra. To verify this hypothesis, the local structure of AsO_4 tetrahedra retained on ferrihydrite surfaces is compared to that of FeO_4 tetrahedra in ferrihydrite extracted using CrystalMaker, version 2.2.4.[58] As listed in Table 2, the R_{As-O} value (1.71 Å) in AsO_4 tetrahedra is slightly shorter (~10%) than the mean R_{Fe-O} value (1.91 Å) in FeO_4 tetrahedra. In addition, the R_{As-O-O} (3.11 Å) and R_{As-Fe} (3.30 Å) values in the second and third coordination shells are well comparable to the R_{Fe-O-O} (3.08 Å) and R_{Fe-Fe} (3.38 Å) values in ferrihydrite. Under such circumstances, the AsO_4 tetrahedra can be possibly incorporated into the crystalline structure of ferrihydrite by substituting the FeO_4 tetrahedra.

CONCLUSION

This work reported the distribution trends and enrichment mechanisms of As and Mo in the HG ferromanganese nodules. According to the XAS analyses, positively charged ferrihydrite and negatively charged δ-MnO_2 were identified to the host phases of As and Mo, respectively. These results were inconsistent with those proposed earlier from the sequential extraction approach, indicating the potential risk of adopting the latter to identify the distribution of As and Mo in natural ferromanganese oxides. In addition, the inner-sphere surface complexation of Mo on δ-MnO_2 and As on ferrihydrite as well as the potential incorporation of AsO_4 into the ferrihydrite structure (Figure 9) highlighted the importance of specific chemical binding toward their immobilization. The identification of As and Mo distribution and speciation in the HG ferromanganese nodules would help predict their migration and fate in the corresponding marine environment. In view of the different mineralogical constituents of HG, DG, and HT ferromanganese oxides, additional studies are still required to further distinguish the enrichment mechanisms of trace elements in various natural ferromanganese samples with disparate origins.

AUTHOR INFORMATION

Corresponding Authors

*Telephone/Fax: +81-3-5841-4506. E-mail: shitongyang-dmn@outlook.com.
*Telephone/Fax: +81-3-5841-4506. E-mail: ytakaha@eps.s.u-tokyo.ac.jp.

ORCID

Shitong Yang: 0000-0002-3083-5485
Haibo Qin: 0000-0002-7404-3703
Masato Tanaka: 0000-0002-6454-7115
Minako Kurisu: 0000-0002-3251-4757

Notes

The authors declare no competing financial interest.

DOI: 10.1021/acsearthspacechem.8b00119
ACS Earth Space Chem. 2019, 3, 29−38

■ ACKNOWLEDGMENTS

This work was supported by the Japan Society for the Promotion of Science (JSPS) Grant-in-Aid for Scientific Research (KAKENHI, Grants 17H04582 and 17H06458) and the National Natural Science Foundation of China (U1732132). The authors also acknowledged the funding support from "Scientific Research on Genesis of Marine Resources" for "Next-Generation Technology for Ocean Resources Exploration (ZIPANG in Ocean)", as a part of the "Cross-Ministerial Strategic Innovation Promotion Program (SIP)" of the Japanese government. The XANES and EXAFS measurements were performed with the approval of SPring-8/JASRI (Proposals 2015A0118, 2016A0127, and 2018A0148) and KEK (Proposals 2014G058 and 2015G664).

■ REFERENCES

(1) Takahashi, Y.; Manceau, A.; Geoffroy, N.; Marcus, M. A.; Usui, A. Chemical and structural control of the partitioning of Co, Ce, and Pb in marine ferromanganese oxides. *Geochim. Cosmochim. Acta* **2007**, *71*, 984−1008.

(2) Kashiwabara, T.; Takahashi, Y.; Marcus, M. A.; Uruga, T.; Tanida, H.; Terada, Y.; Usui, A. Tungsten species in natural ferromanganese oxides related to its different behavior from molybdenum in oxic ocean. *Geochim. Cosmochim. Acta* **2013**, *106*, 364−378.

(3) Kashiwabara, T.; Oishi, Y.; Sakaguchi, A.; Sugiyama, T.; Usui, A.; Takahashi, Y. Chemical processes for the extreme enrichment of tellurium into marine ferromanganese oxides. *Geochim. Cosmochim. Acta* **2014**, *131*, 150−163.

(4) Nozaki, T.; Tokumaru, A.; Takaya, Y.; Kato, Y.; Suzuki, K.; Urabe, T. Major and trace element compositions and resource potential of ferromanganese crust at Takuyo Daigo Seamount, northwestern Pacific Ocean. *Geochem. J.* **2016**, *50*, 527−537.

(5) Bodin, S.; Godet, A.; Matera, V.; Steinmann, Ph.; Vermeulen, J.; Gardin, S.; Adatte, T.; Coccioni, R.; Föllmi, K. B. Enrichment of redox-sensitive trace metals (U, V, Mo, As) associated with the late Hauterivian Faraoni oceanic anoxic event. *Int. J. Earth Sci.* **2007**, *96*, 327−341.

(6) Hein, J. R.; Koschinsky, A.; Halliday, A. N. Global occurrence of tellurium-rich ferromanganese crusts and a model for the enrichment of tellurium. *Geochim. Cosmochim. Acta* **2003**, *67*, 1117−1127.

(7) Koschinsky, A.; Hein, J. R. Uptake of elements from seawater by ferromanganese crusts: Solid-phase associations and seawater speciation. *Mar. Geol.* **2003**, *198*, 331−351.

(8) Marcus, M. A.; Manceau, A.; Kersten, M. Mn, Fe, Zn and As speciation in a fast-growing ferromanganese marine nodule. *Geochim. Cosmochim. Acta* **2004**, *68*, 3125−3136.

(9) Liu, H.; Lu, X. C.; Li, J.; Chen, X. Y.; Zhu, X. Y.; Xiang, W. L.; Zhang, R.; Wang, X. L.; Lu, J. J.; Wang, R. C. Geochemical fates and unusual distribution of arsenic in natural ferromanganese duricrust. *Appl. Geochem.* **2017**, *76*, 74−87.

(10) Calvert, S. E.; Piper, D. Z. Geochemistry of ferromanganese nodules from DOMES Site A, Northern Equatorial Pacific: Multiple diagenetic metal sources in the deep sea. *Geochim. Cosmochim. Acta* **1984**, *48*, 1913−1928.

(11) Shimmield, G. B.; Price, N. B. The behaviour of molybdenum and manganese during early sediment diagenesis—Offshore Baja California, Mexico. *Mar. Chem.* **1986**, *19*, 261−280.

(12) Kashiwabara, T.; Takahashi, Y.; Tanimizu, M.; Usui, A. Molecular-scale mechanisms of distribution and isotopic fractionation of molybdenum between seawater and ferromanganese oxides. *Geochim. Cosmochim. Acta* **2011**, *75*, 5762−5784.

(13) Villalobos, M.; Toner, B.; Bargar, J.; Sposito, G. Characterization of the manganese oxide produced by *pseudomonas putida* strain MnB1. *Geochim. Cosmochim. Acta* **2003**, *67*, 2649−2662.

(14) Foster, A. L.; Brown, G. E.; Parks, G. A. X-ray absorption fine structure study of As(V) and Se(IV) sorption complexes on hydrous Mn oxides. *Geochim. Cosmochim. Acta* **2003**, *67*, 1937−1953.

(15) *Iron Oxides in the Laboratory*; Schwertmann, U., Cornell, R. M., Eds.; Wiley-VCH: Weinheim, Germany, 2000; pp 67−112, DOI: 10.1002/9783527613229.

(16) Koschinsky, A.; Halbach, P. Sequential extraction of marine ferromanganese precipitates: Genetic implications. *Geochim. Cosmochim. Acta* **1995**, *59*, 5113−5132.

(17) Ravel, B.; Newville, M. ATHENA, ARTEMIS, HEPHAESTUS: Data analysis for X-ray absorption spectroscopy using IFEFFIT. *J. Synchrotron Radiat.* **2005**, *12*, 537−541.

(18) Ankudinov, A. L.; Ravel, B.; Rehr, J. J.; Conradson, S. D. Real-space multiple-scattering calculation and interpretation of X-ray-absorption near-edge structure. *Phys. Rev. B: Condens. Matter Mater. Phys.* **1998**, *58*, 7565−7576.

(19) Sholkovitz, E. R. Artifacts associated with the chemical leaching of sediments for rare-earth elements. *Chem. Geol.* **1989**, *77*, 47−51.

(20) Gilmore, E. A.; Evans, G. J.; Ho, M. D. Radiochemical assessment of the readsorption and redistribution of lead in the SM&T sequential extraction procedure. *Anal. Chim. Acta* **2001**, *439*, 139−151.

(21) Peacock, C. L.; Sherman, D. M. Crystal-chemistry of Ni in marine ferromanganese crusts and nodules. *Am. Mineral.* **2007**, *92*, 1087−1092.

(22) Manceau, A.; Lanson, M.; Takahashi, Y. Mineralogy and crystal chemistry of Mn, Fe, Co, Ni, and Cu in a deep-sea Pacific polymetallic nodule. *Am. Mineral.* **2014**, *99*, 2068−2083.

(23) Varentsov, I. M.; Drits, V. A.; Gorshkov, A. I.; Sivtsov, A. V.; Sakharov, B. A. Me−Fe oxyhydroxide crusts from Krylov Seamount (Eastern Atlantic): Mineralogy, geochemistry and genesis. *Mar. Geol.* **1991**, *96*, 53−70.

(24) Manceau, A.; Gorshkov, A. I.; Drits, V. A. Structural chemistry of Mn, Fe, Co, and Ni in manganese hydrous oxides: Part II. Information from EXAFS spectroscopy and electron and X-ray diffraction. *Am. Mineral.* **1992**, *77*, 1144−1157.

(25) Manceau, A.; Lanson, M.; Geoffroy, N. Natural speciation of Ni, Zn, Ba and As in ferromanganese coatings on quartz using X-ray fluorescence, absorption, and diffraction. *Geochim. Cosmochim. Acta* **2007**, *71*, 95−128.

(26) Manceau, A.; Gorshkov, A. I.; Drits, V. A. Structural chemistry of Mn, Fe, Co, and Ni in manganese hydrous oxides: Part I. Information from XANES spectroscopy. *Am. Mineral.* **1992**, *77*, 1133−1143.

(27) Manceau, A.; Drits, V. A. Local structure of ferrihydrite and feroxyhite by EXAFS spectroscopy. *Clay Miner.* **1993**, *28*, 165−184.

(28) Zhu, M. Q.; Ginder-Vogel, M.; Parikh, S. J.; Feng, X. H.; Sparks, D. L. Cation effects on the layer structure of biogenic Mn-oxides. *Environ. Sci. Technol.* **2010**, *44*, 4465−4471.

(29) Zhao, S. L.; Wang, Q.; Sun, J. Y.; Borkiewicz, O. J.; Huang, R. X.; Saad, E. M.; Fields, B.; Chen, S.; Zhu, M. Q.; Tang, Y. Z. Effect of Zn coprecipitation on the structure of layered Mn oxides. *Chem. Geol.* **2018**, *493*, 234−245.

(30) Drits, V. A.; Silvester, E.; Gorshkov, A. I.; Manceau, A. Structure of synthetic monoclinic Na-rich birnessite and hexagonal birnessite: I. Results from X-ray diffraction and selected-area electron diffraction. *Am. Mineral.* **1997**, *82*, 946−961.

(31) Yu, Q. Q.; Tanaka, K.; Kozai, N.; Sakamoto, F.; Tani, Y.; Ohnuki, T. Adsorption of Cs onto biogenic birnessite: Effects of layer structure, ionic strength, and competition cations. *ACS Earth Space Chem.* **2018**, *2*, 797−810.

(32) Finck, N.; Schlegel, M. L.; Bauer, A. Structural iron in dioctahedral and trioctahedral smectites: A polarized XAS study. *Phys. Chem. Miner.* **2015**, *42*, 847−859.

(33) Kéri, A.; Dähn, R.; Krack, M.; Churakov, S. V. Combined XAFS spectroscopy and Ab Initio study on the characterization of iron incorporation by montmorillonite. *Environ. Sci. Technol.* **2017**, *51*, 10585−10594.

DOI: 10.1021/acsearthspacechem.8b00119
ACS Earth Space Chem. 2019, 3, 29−38

(34) Manning, B. A.; Fendorf, S. E.; Bostick, B.; Suarez, D. L. Arsenic(III) oxidation and arsenic(V) adsorption reactions on synthetic birnessite. *Environ. Sci. Technol.* **2002**, *36*, 976−981.
(35) Chen, N.; Jiang, D. T.; Cutler, J.; Kotzer, T.; Jia, Y. F.; Demopoulos, G. P.; Rowson, J. W. Structural characterization of poorly-crystalline scorodite, iron(III)-arsenate coprecipitates and uranium mill neutralized raffinate solids using X-ray absorption fine structure spectroscopy. *Geochim. Cosmochim. Acta* **2009**, *73*, 3260−3276.
(36) Neupane, G.; Donahoe, R. J.; Arai, Y. Kinetics of competitive adsorption/desorption of arsenate and phosphate at the ferrihydrite−water interface. *Chem. Geol.* **2014**, *368*, 31−38.
(37) Wu, Y.; Kukkadapu, R. K.; Livi, K. J. T.; Xu, W. Q.; Li, W.; Sparks, D. L. Iron and arsenic speciation during As(III) oxidation by manganese oxides in the presence of Fe(II): Molecular-level characterization using XAFS, Mössbauer, and TEM analysis. *ACS Earth Space Chem.* **2018**, *2*, 256−268.
(38) Morin, G.; Lecocq, D.; Juillot, F.; Calas, G.; Ildefonse, P.; Belin, S.; Briois, V.; Dillmann, P.; Chevallier, P.; Gauthier, C.; Sole, A.; Petit, P. E.; Borensztajn, S. EXAFS evidence of sorbed arsenic(V) and pharmacosiderite in a soil overlying the Echassières geochemical anomaly, Allier, France. *Bull. Soc. Geol. Fr.* **2002**, *173*, 281−291.
(39) Wu, Y.; Li, W.; Sparks, D. L. Effect of Iron(II) on Arsenic Sequestration by δ-MnO_2: Desorption Studies Using Stirred-Flow Experiments and X-Ray Absorption Fine Structure Spectroscopy. *Environ. Sci. Technol.* **2015**, *49*, 13360−13368.
(40) Guo, Q. H.; Cao, Y. W.; Yin, Z. W.; Yu, Z. Y.; Zhao, Q.; Shu, Z. Enhanced Removal of Arsenic from Water by Synthetic Nanocrystalline Iowaite. *Sci. Rep.* **2017**, *7*, 17546.
(41) Zhang, G. S.; Liu, F. D.; Liu, H. J.; Qu, J. H.; Liu, R. P. Respective role of Fe and Mn oxide contents for arsenic sorption in iron and manganese binary oxide: An X-ray absorption spectroscopy investigation. *Environ. Sci. Technol.* **2014**, *48*, 10316−10322.
(42) Zhu, M. Q.; Paul, K. W.; Kubicki, J. D.; Sparks, D. L. Quantum chemical study of arsenic(III, V) adsorption on Mn-oxides: Implications for arsenic(III) oxidation. *Environ. Sci. Technol.* **2009**, *43*, 6655−6661.
(43) Sherman, D. M.; Randall, S. R. Surface complexation of arsenic(V) to iron(III) (hydr)oxides: Structural mechanism from ab initio molecular geometries and EXAFS spectroscopy. *Geochim. Cosmochim. Acta* **2003**, *67*, 4223−4230.
(44) Neupane, G.; Donahoe, R. J.; Arai, Y. Kinetics of competitive adsorption/desorption of arsenate and phosphate at the ferrihydrite−water interface. *Chem. Geol.* **2014**, *368*, 31−38.
(45) Das, S.; Essilfie-Dughan, J.; Hendry, M. J. Arsenate partitioning from ferrihydrite to hematite: Spectroscopic evidence. *Am. Mineral.* **2014**, *99*, 749−754.
(46) Sowers, T. D.; Harrington, J. M.; Polizzotto, M. L.; Duckworth, O. W. Sorption of arsenic to biogenic iron (oxyhydr)oxides produced in circumneutral environments. *Geochim. Cosmochim. Acta* **2017**, *198*, 194−207.
(47) Scheidegger, A. M.; Sparks, D. L. A critical assessment of sorption−desorption mechanisms at the soil mineral/water interface. *Soil Sci.* **1996**, *161*, 813−831.
(48) Yang, S. T.; Sheng, G. D.; Tan, X. L.; Hu, J.; Du, J. Z.; Montavon, G.; Wang, X. K. Determination of Ni(II) uptake mechanisms on mordenite surfaces: A combined macroscopic and microscopic approach. *Geochim. Cosmochim. Acta* **2011**, *75*, 6520−6534.
(49) James, R. O.; Healy, T. W. Adsorption of hydrolysable metal ions at the oxide−water interface, III. Thermodynamic model of adsorption. *J. Colloid Interface Sci.* **1972**, *40*, 65−81.
(50) Kosmulski, M. pH-dependent surface charging and points of zero charge. IV. update and new approach. *J. Colloid Interface Sci.* **2009**, *337*, 439−448.
(51) Guan, Y.; Sun, X. M.; Jiang, X. D.; Sa, R.; Zhou, L.; Huang, Y.; Liu, Y. T.; Li, X. J.; Lu, R. F.; Wang, C. The effect of Fe−Mn minerals and seawater interface and enrichment mechanism of ore-forming elements of polymetallic crusts and nodules from the South China Sea. *Acta Oceanol. Sin.* **2017**, *36*, 34−46.
(52) Qin, H. B.; Takeichi, Y.; Nitani, H.; Terada, Y.; Takahashi, Y. Tellurium distribution and speciation in contaminated soils from abandoned mine tailings: Comparison with selenium. *Environ. Sci. Technol.* **2017**, *51*, 6027−6035.
(53) Ying, S. C.; Kocar, B. D.; Fendorf, S. Oxidation and competitive retention of arsenic between iron- and manganese oxides. *Geochim. Cosmochim. Acta* **2012**, *96*, 294−303.
(54) Parida, K. M.; Gorai, B.; Das, N. N.; Rao, S. B. Studies on ferric oxide hydroxides III. Adsorption of selenite (SeO_3^{2-}) on different forms of iron oxyhydroxides. *J. Colloid Interface Sci.* **1997**, *185*, 355−362.
(55) Bai, Y. H.; Yang, T. T.; Liang, J. S.; Qu, J. H. The role of biogenic Fe−Mn oxides formed in situ for arsenic oxidation and adsorption in aquatic ecosystems. *Water Res.* **2016**, *98*, 119−127.
(56) Chubar, N.; Gerda, V.; Szlachta, M. Mechanism of selenite removal by a mixed adsorbent based on Fe−Mn hydrous oxides studied using X-ray absorption spectroscopy. *Environ. Sci. Technol.* **2014**, *48*, 13376−13383.
(57) Michel, F. M.; Ehm, L.; Antao, S. M.; Lee, P. L.; Chupas, P. J.; Liu, G.; Strongin, D. R.; Schoonen, M. A. A.; Phillips, B. L.; Parise, J. B. The structure of ferrihydrite, a nanocrystalline material. *Science* **2007**, *316*, 1726−1729.
(58) Gong, Y. X.; Yatongchai, C.; Wren, A. W.; Mellott, N. P. Reintroducing sborgite: Crystallization through exposure of sodium borosilicate glasses to moisture. *Mater. Lett.* **2014**, *136*, 265−270.

DOI: 10.1021/acsearthspacechem.8b00119
ACS Earth Space Chem. 2019, 3, 29−38